1521-009X/47/10/1174–1182$35.00
Drug Metabolism and Disposition

https://doi.org/10.1124/dmd.119.086967
Drug Metab Dispos 47:1174–1182, October 2019

Special Section on Pharmacokinetic and Drug Metabolism Properties of Novel Therapeutic Modalities

Plasma and Liver Protein Binding of *N*-Acetylgalactosamine–Conjugated Small Interfering RNA

Sara C. Humphreys, Mai B. Thayer, Julie M. Lade, Bin Wu, Kelvin Sham, Babak Basiri, Yue Hao, Xin Huang, Richard Smith, and Brooke M. Rock

Pharmacokinetics and Drug Metabolism Department, Amgen Research, South San Francisco, California (S.C.H., M.B.T., J.M.L., B.B., R.S., B.M.R.); Hybrid Modality Engineering Department, Amgen Research, Thousand Oaks, California (B.W., K.S.); and Molecular Engineering Department, Amgen Research, Cambridge, Massachusetts (Y.H., X.H.)

Received February 22, 2019; accepted May 6, 2019

ABSTRACT

Understanding small interfering RNA (siRNA) fraction unbound (f_u) in relevant physiologic compartments is critical for establishing pharmacokinetic-pharmacodynamic relationships for this emerging modality. In our attempts to isolate the equilibrium free fraction of *N*-acetylgalactosamine–conjugated siRNA using classic small-molecule in vitro techniques, we found that the hydrodynamic radius was critical in determining the size exclusion limit requirements for f_u isolation, largely validating the siRNA "rigid rod" hypothesis. With this knowledge, we developed an orthogonally validated 50 kDa molecular-mass cutoff ultrafiltration assay to quantify f_u in biologic matrices including human, nonhuman primate, rat, and mouse plasma, and human liver homogenate. To enhance understanding of the siRNA-plasma interaction landscape, we examined the effects of various common oligonucleotide therapeutic modifications to the ribose and helix backbone on siRNA f_u in plasma ($f_{u,plasma}$) and found that chemical modifications can alter plasma protein binding by at least 20%. Finally, to gain insight into which specific plasma proteins bind to siRNA, we developed a qualitative screen to identify binding "hits" across a panel of select purified human plasma proteins.

Introduction

Fraction unbound (f_u) is a measure of free drug at equilibrium in a biologic matrix of interest. In this paper, we describe methods to quantify small interfering RNA (siRNA) f_u in plasma [$f_{u,plasma}$; commonly referred as plasma protein binding (PPB)] and liver tissue homogenate ($f_{u,liver}$). Fraction unbound is routinely quantified for small-molecule therapeutic candidates according to the free drug hypothesis, wherein only the unbound fraction of drug is available to exhibit pharmacologic effects (Rowland et al., 2011). However, the role, if any, of f_u on the pharmacokinetic-pharmacodynamic (PK-PD) relationship has yet to be established for therapeutic siRNA.

siRNA is a rapidly emerging therapeutic modality, with the first US Food and Drug Administration (FDA) approval granted in August 2018 (Hoy, 2018). Although oligonucleotide therapeutics such as siRNA are generally treated as small molecules for regulatory filings, the FDA has not issued any specific guidance around the reporting of in vitro absorption, distribution, metabolism, and excretion properties (e.g., PPB) on this modality to date. While $f_{u,plasma}$ has been described for antisense oligonucleotide (ASO) therapeutics using 30 kDa molecular-weight cutoff (MWCO) ultrafiltration, a corresponding assay has not yet been described for siRNA (Watanabe et al., 2006). For small molecules, $f_{u,plasma}$ is typically measured via ultracentrifugation, ultrafiltration, or equilibrium dialysis. In these assays, the molecular size, shape, mass, and/or density of the small molecule relative to the plasma protein milieu largely determine its differential partitioning based on sedimentation velocity (ultracentrifugation) or porous membrane exclusion limits (ultrafiltration and equilibrium dialysis). For siRNA f_u isolation, the larger size of siRNA [approximately 15 kDa with triantennary *N*-acetylgalactosamine (GalNAc) conjugation] needed to be taken into consideration.

In this publication, we report an orthogonally validated 50 kDa MWCO ultrafiltration assay to quantify $f_{u,plasma}$ and $f_{u,liver}$ of a therapeutic siRNA in human matrices at clinically relevant concentrations and across relevant preclinical species ($f_{u,plasma}$ only). The 21-mer double-stranded siRNA used throughout the study, referred to as siRNA-X, is chemically modified RNA with phosphorothioate (PS) bonds, 2′*O*-methyl (2′-OMe) and 2′deoxy 2′-fluoro (2′-F) ribose modifications, and GalNAc conjugation. PS bonds replace specific

All authors are employees and stock holders of Amgen, Inc.
https://doi.org/10.1124/dmd.119.086967.
This article has supplemental material available at dmd.aspetjournals.org.

ABBREVIATIONS: ASGPR, asialoglycoprotein receptor; ASO, antisense oligonucleotide; BLI, biolayer interferometry; bn-siRNA, biotinylated siRNA; CHAPS, 3-[(3-cholamidopropyl)dimethylammonio]-1-propanesulfonate hydrate; dsRNA, double-stranded RNA; 2′-F, 2′deoxy 2′-fluoro; FDA, Food and Drug Administration; GalNAc, *N*-acetylgalactosamine; MW, molecular weight; MWCO, molecular-weightcutoff; 2′-OMe, 2′*O*-methyl; pAb, polyclonal antibody; PBST, PBS with Tween-20; PK-PD, pharmacokinetic-pharmacodynamic; PPB, plasma protein binding; PS, phosphorothioate; RISC, RNA-induced silencing complex; siRNA, small interfering RNA.

phosphodiester bonds to increase exonuclease resistance (Braasch et al., 2004), 2′-OMe and 2′-F enhance both stability and RNA-induced silencing complex (RISC) interactions (Allerson et al., 2005; Choung et al., 2006), and GalNAc enables targeted hepatocyte uptake via the asialoglycoprotein receptor (ASGPR) (Foster et al., 2018; Janas et al., 2018; Springer and Dowdy, 2018). siRNA-X is highly efficacious, eliciting greater than 80% target mRNA and protein knockdown over at least three months after a single 3-mg/kg dose in nonhuman primates (manuscript in preparation). Numerous chemical modifications and ligands used in the current generation of oligonucleotide therapeutics—namely, ASO therapeutics—have been demonstrated to alter the extent of protein binding (Wilce et al., 2012; Geary et al., 2015; Bhandare and Ramaswamy, 2016; Juliano, 2016; Schirle et al., 2016; Bailey et al., 2017; Gaus et al., 2018). To understand how RNA modifications and ligand conjugation affect siRNA PPB specifically, we investigated the effects of PS, 2′-OMe, 2′-F, GalNAc, and biotin on $f_{u,plasma}$.

Protein-siRNA interactions may affect siRNA tissue clearance, macroscopic (tissue-level) and microscopic (cell-level) distribution, and/or pharmacological activity; conversely, binding of siRNA to certain proteins may change the function or fate of those proteins. Taken together, these works, addressing both total siRNA-matrix interactions to inform the former and screening for specific siRNA-protein interactions to inform the latter, provide a set of complementary tools to begin to establish the role and the relevance of protein binding for this emerging modality. Furthermore, while the extent of total PPB at equilibrium is of interest from a PK-PD modeling perspective, knowledge of interactions between therapeutic siRNA and specific plasma proteins may help identify potential off-target protein-binding liabilities, drug-drug interactions, and aid the design of next-generation siRNA molecules.

Materials and Methods

Materials

All oligonucleotides were synthesized in house using commercially available reagents or purchased from Integrated DNA Technologies (Skokie, IL). Human plasma protein [albumin (#A3782), α-1-acid glycoprotein (#G9885), α-2-macroglobulin (#SRP6314), fibronectin (#F2006), fibrinogen (#F3879), haptoglobin (#372022), IgG Fc fragment (#AG714)] buffer reagents, and Amicon Ultra 0.5-ml centrifugal filters [30 kDa MWCO (#UFC503008) and 50 kDa MWCO (#UFC505008)] were obtained from Millipore Sigma (Burlington, MA). Slide-A-Lyzer 0.5-ml MINI Dialysis Devices (20 kDa MWCO; #88402) were obtained from Thermo Fisher (Waltham, MA). α-thrombin was obtained from MP Biomedicals (#02194918; Santa Ana, CA). All plasma (K2 EDTA treated) and liver tissues were obtained from BioIVT (Westbury, NY). All plasma samples were from frozen pooled, mixed-gender donors from CD-1 mice (MSEPLEDTA2; 300 donors), cynomolgus monkeys (CYNPLEDTA2; 22 donors), Sprague-Dawley rats (RATPLEDTA2; 60 donors), and humans (HMPLEDTA2; 69 donors). Human liver tissue was from three pooled, female donors (aged 30–40 years) and homogenized (from frozen) in Tissue Extraction Reagent I (#FNN071; Invitrogen, Carlsbad, CA). Blocking reagents were sourced as follows: heparin (#84020), bovine serum albumin (#A9418), gelatin (#9000-70-8), 3-[(3-cholamidopropyl)dimethylammonio]-1-propanesulfonate hydrate (CHAPS; #C3023), and spermidine (#S2626) from Sigma-Aldrich (St. Louis, MO); I-Block (#T2015) from Invitrogen; and Tween-20 (#85113), Blocking Reagent (#11096176001), and Triton X-100 (#28314) from Thermo Fisher. siRNA-specific rabbit polyclonal antibody (pAb) was generated by Lampire Biologic Laboratories (Encinitas, CA) by immunization of rabbits with siRNA-X.

Methods

Time to Equilibrium of siRNA Binding to Human Plasma by Biolayer Interferometry. Biotinylated siRNA (biotin conjugated to the 3′ terminus of the sense strand; bn-siRNA) in buffer A [10 mM Tris (pH 7.4), 150 mM NaCl, 1 mM $CaCl_2$, 1% gelatin (w/v), 0.13% Triton X-100 (w/v)] was loaded onto pre-equilibrated high-precision streptavidin biosensors (ForteBio LLC, Fremont, CA) to obtain a response of ~1 nm over 1000 seconds. bn-siRNA–loaded tips were rinsed in buffer A for 1 minute, followed by exposure to a five-point (plus two blanks), 3-fold dilution series of human plasma in buffer A [top concentration: 3.3% human plasma in buffer A (v/v)] over 10 minutes. Data were collected on a ForteBio Octet-384 instrument, and analysis and fitting were performed using the ForteBio software (version 10.0).

$f_{u,plasma}$ and $f_{u,liver}$ Determination by Ultrafiltration. To prepare the Ultracel regenerated cellulose filters for use, residual glycerin was removed by twice adding 0.5 ml of phosphate-buffered saline [PBS; 137 mM NaCl, 2.7 mM $CaCl_2$, 10 mM Na_2HPO_4, 1.8 mM KH_2PO_4 (pH 7.4)] and spinning in a bench-top centrifuge for 10 minutes at 3000*g*. The remaining PBS was removed before adding 0.5 ml of PBS with 0.1% Tween-20 (w/v; PBST) and repeating the spin to prevent nonspecific binding of drug to the filter. PBST was removed from the filter and collection tube immediately prior to sample addition (take care to avoid drying the filter). Samples were prepared by spiking known siRNA or small-molecule concentrations into neat plasma or tissue homogenate (pre-equilibrated to 37°C) and incubated at 37°C for 30 minutes, shaking at 500 rpm. A 500-μl sample was transferred into prepared filters and spun at 1500*g* until no more than 20% of the volume had passed through the filter. Only a small volume of ultrafiltrate should be collected, as the protein concentration in the upper reservoir rises during the filtration process (Zeitlinger et al., 2011). To mitigate matrix effects, after ultrafiltration, all donor samples were pretreated with an equivalent volume of PBST, and all ultrafiltrate receiver samples were pretreated with an equivalent volume of plasma/homogenate (standard curves were treated the same way). To measure recovery, drug-spiked PBST controls were performed at every concentration tested. During method development, we set an arbitrary cutoff of 80% recovery in buffer at each concentration tested to ensure that the corresponding f_u readout in plasma or homogenate was representative of the majority of siRNA in the sample. Ultracentrifugation and equilibrium dialysis methods are provided in the Supplemental Methods.

siRNA Detection and Quantitation via 96-Well Plate-Based Hybridization Assay. Sheep anti-digoxigenin polyclonal antibody (#11222089001; Roche) was conjugated with a ruthenium label using the MSD GOLD Sulfo-Tag NHS-Ester conjugation kit (#R31AA-1; Meso Scale Diagnostics, Rockville, MD). Standards and sample buffer were made as follows: 10 mM Tris-HCl (pH 8.0) and 1 mM EDTA. Hybridization buffer was made as follows: 60 mM Na2PO4 (pH 7.0, dibasic), 1 M NaCl, 5 mM EDTA, and 0.02% Tween-20. Lyophilized oligonucleotide probes were custom synthesized from Qiagen Inc. (Hilden, Germany). Sequence-specific capture and detection probes were conjugated to biotin and digoxigenin, respectively. All chemicals and reagents were analytical grade or higher, if not specified.

Test article standard curves were prepared in PBS or plasma at a concentration range of 2.6–166 pM (0.04–2500 ng/ml). The standard curves and samples were diluted 1:10 in sample buffer and added to a 96-well polymerase chain reaction plate to a final volume of 50 μl. Both sequence-specific capture and detection probes were added to hybridization buffer to a final concentration of 50 nM, and 50 μl was added to the samples in buffer. Sample and probes were hybridized in a thermal cycler under the following conditions: 90°C for 5 minutes, 35°C for 30 minutes, and a final hold at 12°C. After hybridization, samples were transferred to an MSD GOLD 96-well Streptavidin SECTOR PR plate (#L13SA; Meso Scale Diagnostics) for 30 minutes at room temperature. Plates were washed and incubated for 1 hour with 50 μl of 2 μg/ml ruthenium-labeled anti-digoxigenin antibody in SuperBlock T20 TBS Blocking Buffer (#37536; Thermo Fisher). After a final wash, 150 μl of MSD Read Buffer T (#R92TD; Meso Scale Diagnostics) was added, and the plate was read in an MSD Sector S 600 instrument (Meso Scale Diagnostics).

Quantitation was performed against standard curves by nonlinear four parameter logistic regression using GraphPad Prism (version 7.04). For ultrafiltration and equilibrium dialysis, percentage recovery (% recovery) in buffer was calculated using eq. 1:

$$\%\ \text{recovery (buffer)} = \frac{[\text{receiver}]}{[\text{donor}]} \times 100 \quad (1)$$

where [donor] is the concentration of siRNA in buffer before addition to the apparatus, and [receiver] is the concentration of siRNA recovered in the ultrafiltrate or on the other side of the dialysis membrane, respectively. The f_u was calculated using eq. 2:

$$f_u = \frac{[\text{receiver}]}{[\text{donor}]}. \quad (2)$$

Dilution of human liver tissue in homogenization buffer was accounted for using eq. 3 (Kalvass et al., 2007):

$$\text{undiluted } f_u = \frac{1/D}{1/f_{u,\text{measured}} - 1/D} \quad (3)$$

where D is the dilution factor.

Comparative Liquid Chromatography–Tandem Mass Spectrometry Analysis of Small-Molecule $f_{u,plasma}$ and $f_{u,liver}$ via Ultracentrifugation and Ultrafiltration. Liquid chromatography–tandem mass spectrometry was used to quantify post-50 kDa MWCO ultrafiltration and ultracentrifugation of warfarin, antipyrine, and timolol in human plasma and rosuvastatin in human liver homogenate (see Supplemental Methods for ultracentrifugation $f_{u,plasma}$ and $f_{u,liver}$ method). Samples were quenched with 40% acetonitrile in water and spun for 10 minutes at 4000*g* before injection on a Kinetex C18 column (2.6 μm, 50 × 2.1 mm; Phenomenex) using a Shimadzu ultrafast liquid chromatography system coupled to an AB Sciex Qtrap 4500 mass spectrometer with a source temperature of 550°C and an ion spray voltage of 4500 V. The mobile phases consisted of 0.1% formic acid in water (mobile phase A) and 0.1% formic acid in acetonitrile (mobile phase B) using a flow rate of 1 ml/min and a gradient as follows: 5% B for 0.8 minutes, 99% B for 0.5 minutes, and return to 5% B to 1.5 minutes. Analytes were detected in positive ion mode using multiple reaction monitoring (Q1→Q3; collision energy, V): warfarin (309.0→163.0 m/z; 20 V), timolol (317.0→261.1 m/z; 25 V), antipyrine (189.1→161.1 m/z; 25 V), rosuvastatin (482.4→258.1 m/z; 45 V), and internal standard tolbutamide (309.0→163.0 m/z; 25 V). Compound peak areas were integrated using Analyst 1.6.2 software (Sciex) and normalized to the internal standard.

Binding of Select Purified Human Plasma Proteins to Biotinylated siRNA-X ± GalNAc. Binary siRNA–protein interactions were measured by biolayer interferometry (BLI) with biotin-conjugated siRNA immobilized on streptavidin tips. bn-siRNA-X (100 nM in buffer A) with or without GalNAc was loaded onto streptavidin BLI tips over 10 minutes to ~2 nm. Loaded tips were rinsed in buffer for 1 minute, then introduced to 1:2 titrations of anti-siRNA pAb antibody (positive control), α-2-macroglobulin, α-thrombin, fibrinogen, fibronectin, albumin, α1-acid glycoprotein, α1-antitrypsin, haptoglobin, and IgG Fc fragment, starting at 1 μM (except the anti-siRNA pAb control at 0.2 μM, and α-2-macroglobulin, α-thrombin, fibrinogen, fibronectin at 0.5 μM). Association and dissociation steps were performed for 10 minutes each.

Results

Time to Equilibrium and Quasi-Kinetic Binding Analysis Using Biolayer Interferometry. Determination of f_u requires that the system be at equilibrium (Schmidt et al., 2010). BLI was used to measure the time taken for biotin-conjugated siRNA-X loaded onto streptavidin tips to reach steady state (Fig. 1). We observed that time to steady state decreased with increasing plasma concentrations, and at 3.3% plasma the system approached equilibrium in 10 minutes. Based on this result and liquid chromatography–mass spectrometry evidence that siRNA-X is stable in plasma for more than 30 minutes (Supplemental Fig. 1), we determined that 30 minutes was sufficient for accurate f_u determination in neat plasma. It is important to recognize that, for all PPB experiments, small molecules included, a compromise must be made to balance time to equilibrium with metabolic stability. Given that the rate of equilibration depends on the ligand-protein complex half-life ($t_{1/2}$; Corzo, 2006), the sensorgrams do not appear to be approaching zero in the dissociation phase, and that plasma is a highly heterogeneous mixture of proteins, it is possible that a population of plasma proteins that bind siRNA tightly have not reached equilibrium in 30 minutes. Therefore, to ensure reproducibility, it is essential to perform the experiment with strict adherence to the 30-minute equilibration time and temperature (37°C).

Comparison of Classic Small-Molecule PPB Methods to Determine the Unbound Fraction of siRNA in Plasma. At roughly 15 kDa, GalNAc-conjugated siRNA is significantly larger than a typical small molecule. Consequently, isolation of the unbound fraction by a semipermeable physical barrier (ultrafiltration and equilibrium dialysis) or by differential sedimentation (ultracentrifugation) requires some adaption from small-molecule f_u isolation methods. Initially, we tested ultrafiltration and equilibrium dialysis devices with 30 and 20 kDa MWCO exclusion limits, respectively, based on commercial availability of devices with MWCOs close to, but greater than, 15 kDa. For ultracentrifugation, owing to complexities of achieving differential sedimentation of similarly sized macromolecular species (Hughes et al., 1938), we elected to test our existing ultracentrifugation small-molecule protocol without modification. We ran initial tests in protein-free medium to ensure that siRNA could freely diffuse across the semipermeable membrane (ultrafiltration and equilibrium dialysis) or would remain in the supernatant after spinning (ultracentrifugation).

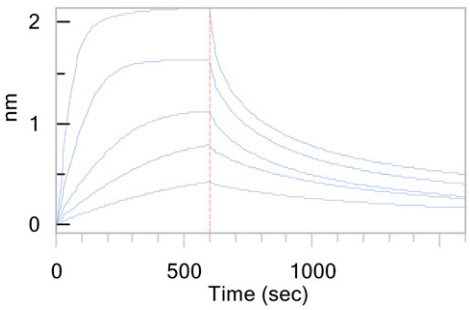

Fig. 1. Representative time to equilibrium of siRNA binding to total human plasma. Reference tip-subtracted sensorgrams depicting a titration of total human plasma interacting with biotinylated siRNA on streptavidin tips. Top plasma concentration is 3.3% (v/v) in buffer A followed by a 1:2 dilution series.

Table 1 shows representative percentage recoveries of 1 μM siRNA-X in PBST in the receiver compartment (ultrafiltration and equilibrium dialysis) or supernatant (ultracentrifugation) for the three techniques. The recoveries—0.0062%, 5.5%, and 24.8% for ultracentrifugation (small-molecule method), equilibrium dialysis (20 kDa MWCO), and ultrafiltration (30 kDa MWCO), respectively—were too low for use in siRNA f_u determination. At first, we hypothesized that the poor recovery was due to nonspecific surface binding to filters, dialysis membranes, and ultracentrifugation tubes. We explored a range of potential blocking reagents, including heparin, alternative siRNA molecules, bovine serum albumin, gelatin, I-Block, spermidine, Blocking Reagent, and Triton X-100. None of the blocking agents tested improved recovery over PBST, and several of them, including heparin, alternative siRNA, and spermidine, significantly reduced the sensitivity of the hybridization detection assay, potentially due to charge-based competition for the capture and detection probes. We subsequently discovered that the pore size of the permeable membrane was the largest determinant for recovery, as we recovered 92% of 1 μM siRNA-X in the receiver compartment of a filtration device with a 50 kDa MWCO in PBST. While this recovery represented a great improvement compared with where we started, recovery can be further improved with optimization of blocking reagents, filter-blocking routines, and centrifugation speeds. We did investigate the effect of replacing PBST with PBS with 0.1% CHAPS (w/v) and found that it significantly improved recovery of asymmetric [larger hydrodynamic radius (R_h)] GalNAc-siRNA molecules (Supplemental Fig. 2). It is important to note that Watanabe et al. (2006) reported over 90% recovery of a fully phosphorothioated 20-mer DNA ASO using a 30 kDa MWCO ultrafiltration method, highlighting that single-stranded DNA and double-stranded RNA (dsRNA) likely differ significantly in their structural conformations.

Akin to ultracentrifugation approaches to measure small-molecule f_u, the ultrafiltration technique described here is likely subject to minor equilibrium perturbation effects as a consequence of the extent and duration of the centrifugal force applied. siRNA-protein interactions most affected by this are weak binders. To ensure reproducible and comparable results using this technique, we recommend using the centrifugation speeds and times described here.

TABLE 1

Comparison of percentage of siRNA-X recovery using different f_u isolation techniques

f_u Isolation Method	MWCO	% Recovery
	kDa	
Ultracentrifugation	n/a	0.0062 ± 0.0003
Equilibrium dialysis	20	5.53 ± 7.13
Ultrafiltration	30	24.7 ± 1.40
Ultrafiltration	50	92.4 ± 11.6

Validation of siRNA R_h via Calculation from Literature Values and siRNA-X Crystal Structure. After observing that a 50 kDa MWCO exclusion limit was required for adequate recovery of siRNA-X across an ultrafiltration apparatus in buffer (Table 1), we realized that R_h, and not molecular weight (MW), governs filter selection (these filters are typically designed for protein-based applications).

siRNA R_h can be calculated using helical rise per base pair from literature values describing dsRNA A-form helix dimensions (Supplemental Calculations 1; Taylor et al., 1985; Baeyens et al., 1995). Initially, we were concerned that backbone and ribose modification of siRNA might cause deviations from the A-form helix structure; however, a crystal structure of siRNA-X confirmed the "rigid rod" linear geometry of siRNA, as well as the A-form helix (helical rise: 0.26–0.29 nm/base pair; R_h: ~2.7–3 nm; Fig. 2B; manuscript in preparation). Consequently, we used literature values of known protein R_h versus protein MW to establish a correction factor to determine siRNA-protein MW equivalence (Fig. 6R_h calculations shown in Supplemental Calculations 2). The 21-mer siRNA-X is roughly equivalent to a 48 kDa protein, which is why it requires a 50 kDa MWCO filter.

Orthogonal Validation of a 50 kDa MWCO Ultrafiltration Method for siRNA-X f_u Determination Using Electrophoretic Mobility Shift Assay and Liquid Chromatography–Mass Spectrometry. Increasing the ultrafiltration MWCO from 30 to 50 kDa resulted in a significant buffer recovery increase, leading us to realize the importance of using of siRNA hydrodynamic radius (R_h) rather than MW in determining which device to use for f_u determination (Table 1). However, given that human plasma consists of a highly heterogeneous mixture of proteins, many of which are 50 kDa or less, it was important to test whether the "unbound fraction" of siRNA in the receiver compartment of the ultrafiltration device was the true f_u or a mixture of unbound siRNA and siRNA bound to small proteins. We ran an electrophoretic mobility shift assay on the ultrafiltrate of 1 μM siRNA-X spiked into human plasma and observed two bands—one consistent with siRNA-X, the other consistent with albumin (Supplemental Fig. 3A). Further testing of the albumin band in plasma without siRNA-X showed that albumin, or some compound that comigrates with albumin, stains with SYBR Gold (Supplemental Fig. 3B); we later demonstrate that albumin does not bind siRNA-X using BLI (Supplemental Fig. 6). Together, these findings suggest that the clear majority of siRNA-X that passes through the 50 kDa MWCO filter is unbound.

Next, to determine whether the 50 kDa MWCO ultrafiltration method was a reliable measure of f_u, we tested it on a panel of small molecules with well established $f_{u,plasma}$ and $f_{u,liver}$ values ranging from majority bound (warfarin) to majority unbound (antipyrine). Table 2 provides a comparison of the reference f_u values obtained using classic PPB methods compared with the 50 kDa MWCO ultrafiltration method. Warfarin $f_{u,plasma}$ was overestimated approximately 4-fold. This is likely because warfarin binds to albumin, and we showed with electrophoretic mobility shift assay that some fraction of albumin is recovered in the receiver compartment using the 50 kDa MWCO filter (Supplemental Fig. 3); the manufacturer also only reports >95% bovine serum albumin retention on these devices (http://www.emdmillipore.com/US/en/life-science-research/protein-sample-preparation/protein-concentration/amicon-ultra-centrifugal-filters/http://www.emdmillipore.com/US/en/product/Amicon-Ultra-0.5mL-Centrifugal-Filters-for-DNA-and-Protein-Purification-and-Concentration,MM_NF-C82301). Recovery of some quantity of albumin is expected given its high abundance,.Its MW (~66 kDa) is sufficiently close to 50 kDa, the filter pore sizes represent a distribution at best, and albumin is not a perfect sphere. Rosuvastatin $f_{u,liver}$ ($f_{u,liver}$ = 0.14) was underestimated relative to the literature values ($f_{u,liver}$ = 0.23), which were generated using equilibrium dialysis (Pfeifer et al., 2013). This is likely because applying centrifugal force to homogenate results in blocking of the filtration pores to some extent. Lowering the centrifugation speed could minimize this effect, or this problem could be avoided entirely with equilibrium dialysis.

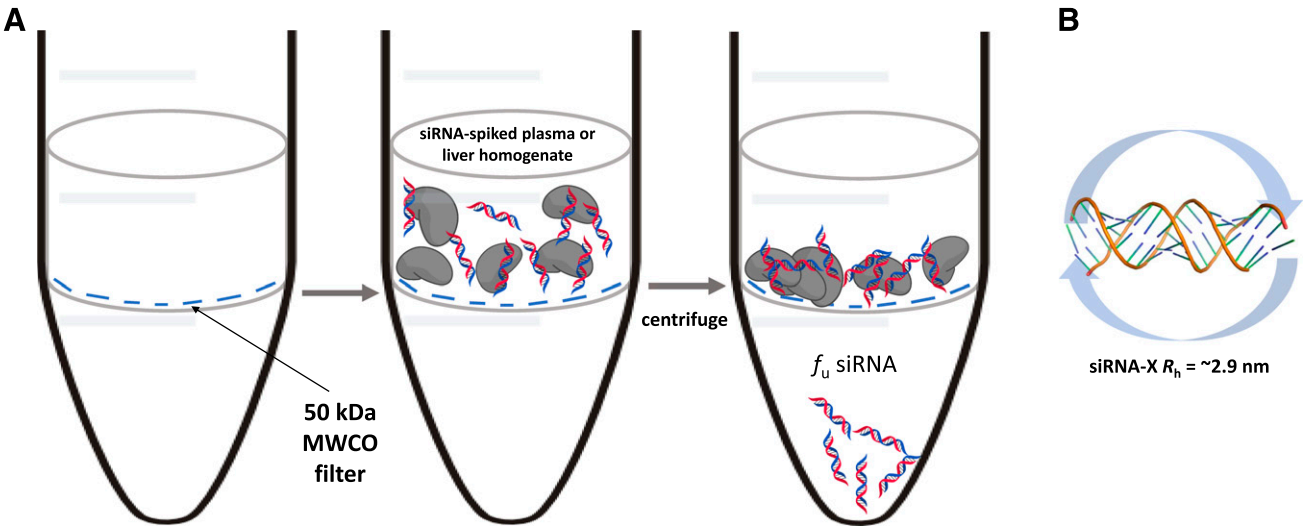

Fig. 2. (A) Workflow of determination of siRNA f_u via ultrafiltration. Step 1: pretreat filter with detergent-containing buffer [we found that PBST (Table 1) and PBS+CHAPS (Supplemental Fig. 2) provided good recovery with a 50 kDa MWCO filter]. Step 2: add pre-equilibrated siRNA-spiked matrix into donor compartment of filter and centrifuge. Step 3: collect flow-through and quantify siRNA f_u. (B) Depiction of siRNA-X R_h based on the crystal structure.

TABLE 2

Validation of 50 kDa MWMCO ultrafiltration method for determination of $f_{u,plasma}$ and $f_{u,liver}$ using well characterized small molecules

SM	Matrix (Human)	f_u (Measured)	f_u (Reference)	Reference Method
Antipyrine	Plasma	0.867 ± 0.110	0.9	Ultracentrifugation
Timolol	Plasma	0.347 ± 0.074	0.4	Ultracentrifugation
Warfarin	Plasma	0.043 ± 0.007	0.01[a]	Ultracentrifugation
Rosuvastatin	Liver homogenate	0.14 ± 0.03	0.23[b]	Equilibrium dialysis

SM, small molecule.
[a]O'Reilly (1972).
[b]Pfeifer et al. (2013); Yoshikado et al. (2017).

Cross-Species Comparison of siRNA PPB. As the development of therapeutic molecules necessitates testing in multiple preclinical species, it is important to understand if PPB properties are consistent across relevant species—in this case, mouse, rat, and cynomolgus monkeys—as well as in humans over a range of therapeutically relevant concentrations. Cross-species PPB comparisons could help at least partly explain any observed differences in PK profiles. A two-way analysis of variance (ANOVA) of the data in Fig. 3A indicated that there was no significant distinction for siRNA-X $f_{u,plasma}$ across the species tested ($P > 0.05$), but that there was an increase in the fraction unbound with increasing concentration from 0.037 to 1 μM ($P < 0.01$). The latter is consistent with PPB data reported across multiple modalities (Schmidt et al., 2010). However, given the limited concentration range, it cannot be determined if PPB is concentration-independent (linear) or concentration-dependent (non-linear), as both cases have been reported (Deitchman et al., 2018). It should be noted that Gaus et al. (2018) recently observed that plasma binding of a 50% phosphorothioated DNA/RNA duplex was ~19-fold higher in monkey plasma compared with humans (mouse and rat were intermediate). This remains an area of active research.

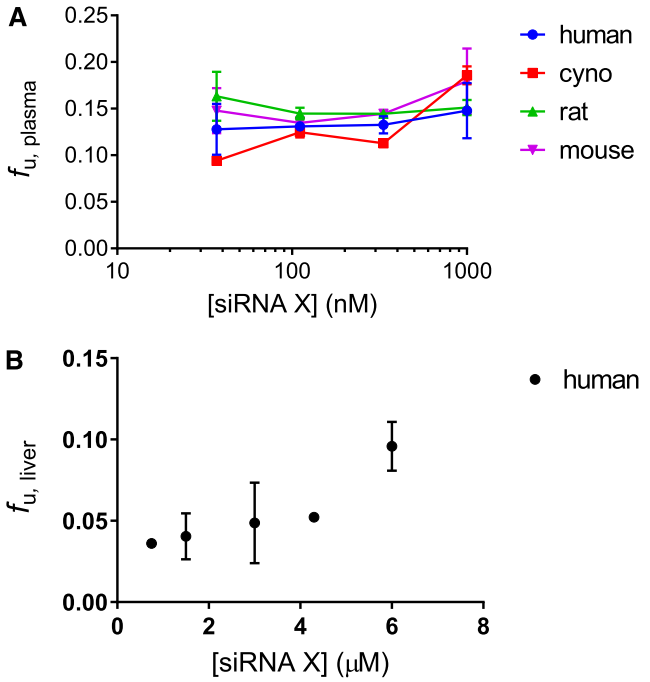

Fig. 3. PPB and liver protein binding of siRNA-X. (A) Cross-species comparison of $f_{u,plasma}$ across a range of therapeutically relevant siRNA concentrations. There was a significant increase in $f_{u,plasma}$ with concentration ($P < 0.01$) that was not dependent on species (determined by two-way ANOVA, GraphPad Prism). (B) siRNA-X $f_{u,liver}$ across a range of therapeutically relevant concentrations. Plasma measurements were performed in triplicate; liver measurements were performed in duplicate.

Determination of siRNA-X $f_{u,liver}$ in Human Liver Tissue Homogenate. Many siRNA molecules currently under investigation as therapeutics, including siRNA-X, are targeted to the liver via GalNAc conjugation, which enables delivery via ASGPR-mediated uptake. It was therefore of interest to measure the unbound fraction in the liver. For small molecule, $f_{u,liver}$ is typically measured by equilibrium dialysis (Pfeifer et al., 2013); however, in the absence of commercially available devices with ~50 kDa MWMCO for siRNA, we adapted the plasma ultrafiltration method described earlier to human liver homogenate (Fig. 3B). For siRNA-X, $f_{u,liver}$ ranged from 0.018 to 0.051 over a therapeutically relevant concentration range (0.375–6 μM), indicating that it is mostly bound in human liver tissue, and that binding was higher in liver homogenate compared with plasma. Over this concentration range, the data did not appear to be strictly linear.

The Effect of Chemical Modifications and Ligand Conjugates on siRNA PPB. To investigate the effect of different chemical modifications on siRNA PPB, we measured $f_{u,plasma}$ on constructs with the same siRNA-X sequence that had been modified to be entirely 2′-OMe, 2′-F, or PS modified (Fig. 4). Consistent with the literature, we observed that PS increases PPB, and 2′-OMe decreases PPB relative to the siRNA-X control (Braasch et al., 2004; Allerson et al., 2005; Choung et al., 2006; Gaus et al., 2018). There was no statistically significant difference between siRNA-X and fully 2′-F siRNA $f_{u,plasma}$. We could not find evidence in the literature discussing the role of 2′-F in siRNA PPB differences; however, in certain ASO cases, 2′-F appears to confer increased specificity and/or affinity to select cytosolic proteins (Shen et al., 2015; Vickers and Crooke, 2016). At 1 μM siRNA, the effects of PS and 2′-OMe appear informative from an siRNA therapeutic design perspective because alterations in the numbers of these modifications could significantly affect the PK profile of siRNA in the blood.

We also looked at the effect of siRNA ligand conjugation on PPB and found that removal of GalNAc increased protein binding, and biotin had no statistically significant effect compared with siRNA-X. The implications of these findings are that conjugating biotin to siRNA as a functional handle does not affect PPB, and that GalNAc may be important for reducing PPB interactions. Furthermore, while siRNA-X $f_{u,plasma}$ was slightly less than $f_{u,serum}$, this result was not statistically significant, indicating that the role of clotting factors in total PPB is minimal. In addition, we ran the same PPB assay on a panel of four other therapeutic candidate siRNA molecules with different sequences and similar modification patterns, and found that at 1 μM siRNA, $f_{u,plasma}$ varied between approximately 0.08 and 0.15, which was significantly less than the effects observed with more extreme modification patterns here (data not shown).

Qualitative Determination of Specific Interactions between siRNA-X and Select Human Plasma Proteins. We used BLI to gain further insight into which specific plasma proteins bound to siRNA-X. We elected to compare binding in the presence and absence of

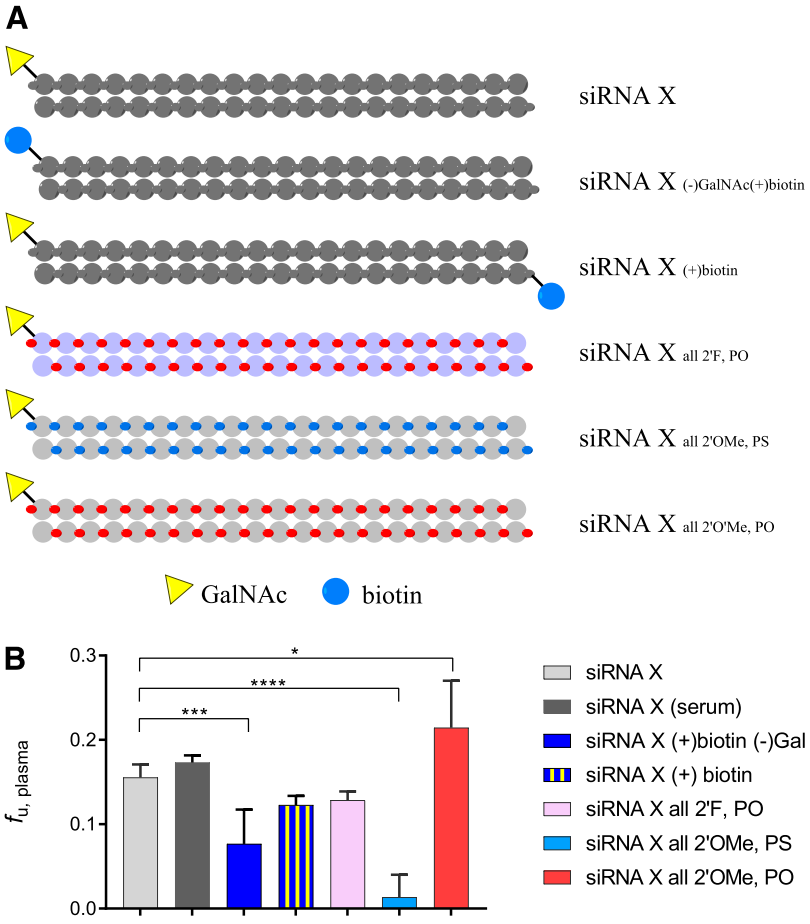

Fig. 4. Effect of chemical modifications on $f_{u,plasma}$ at 1 μM siRNA concentration. (A) Constructs tested with the sense strand depicted at the top (5′-3′) and the complementary antisense strand at the bottom. The RNA base sequence was constant across constructs, with only the conjugated ligand(s) (GalNAc and biotin), the ribose (2′-OMe, 2′-F), and the backbone (PS or phosphodiester) changing. (B) $f_{u,plasma}$ for each of the constructs in plasma; siRNA-X was also measured in serum. Results were compared using an ordinary one-way ANOVA with multiple comparisons in GraphPad Prism. Significant differences between the test article, siRNA-X in plasma, and the other constructs are reported as $*P < 0.05$; $**P < 0.01$; $***P < 0.001$; and $****P < 0.0001$.

GalNAc due to the observation of different trends in total plasma protein binding when GalNAc was present or absent in various constructs (Supplemental Figs. 4 and 5), and because siRNA-X PPB significantly increased when GalNAc was removed (Fig. 4). Selection criteria for panel inclusion was based on plasma abundance [albumin, IgG Fc fragment, fibrinogen, α-2-macroglobulin, α-1-antitrypsin, and haptoglobin (Anderson and Anderson, 2002)], prior evidence of prominent small-molecule or ASO drug binding [albumin, α-1-acid glycoprotein, α-2-macroglobulin (Cossum et al., 1993; Brown et al., 1994; Srinivasan et al., 1995; Watanabe et al., 2006)], or RNA aptamer binding precedence [fibronectin (Ulrich et al., 2002) and α-thrombin (Long et al., 2008)]. An siRNA-specific rabbit pAb was used as a positive control.

α-2-Macroglobulin and α-thrombin bound to both siRNA-X constructs, while fibronectin and fibrinogen bound to bn-siRNA-X (-Gal) only (Fig. 5), and no binding was observed with albumin, α1-acid glycoprotein, α1-antitrypsin, haptoglobin, and IgG Fc (negative results provided in Supplemental Fig. 6) (Fig. 6).

Discussion

We have described and validated an assay to measure the free fraction of GalNAc siRNA in plasma and liver homogenate at equilibrium. The rationale for developing the assay was to gain insight into the protein-binding properties of therapeutic siRNA molecules to support PK-PD modeling efforts and to pre-empt any regulatory filing requests. Under the International Council for Harmonization of Technical Requirements for Pharmaceuticals for Human Use and FDA guidelines, therapeutic siRNA is generally treated as a small molecule, as there is no specific guidance for this emerging modality. Small-molecule regulatory filings typically require in vitro PPB data for preclinical animals and humans [S3A Guidance on Toxicokinetics (https://www.fda.gov/downloads/Drugs/GuidanceComplianceRegulatoryInformation/Guidances/UCM519697.pdf) and M3(R2) Guidance on Nonclinical Safety Studies for the Conduct of Human Clinical Trials and Marketing Authorization for Pharmaceuticals (https://www.fda.gov/downloads/Drugs/GuidanceComplianceRegulatoryInformation/Guidances/UCM073246.pdf)]. To our knowledge, whereas f_u methods have been described for heavily phosphorothioated single-stranded DNA–based ASOs, this is the first description of an siRNA assay (Cossum et al., 1993; Braasch et al., 2004; Watanabe et al., 2006).

siRNA R_h Dictates f_u Separation Requirements. A major finding of this work was that MWCO exclusion limits, which are estimated from approximately spherical globular proteins, cannot be directly applied to siRNA for f_u experiments because siRNA R_h is ~2-fold greater than a protein of equivalent MW . Therefore, to ensure siRNA can diffuse freely across a porous membrane for f_u separation, filters must be selected based on R_h and not MW.

siRNA is hypothesized to exist as a "rigid rod" in solution due to the geometry of the dsRNA A-form helix (Kornyshev and Leikin, 2013; Kozielski et al., 2013; Dandekar et al., 2015). We recently obtained a crystal structure of siRNA-X confirming its linear geometry (R_h = ~2.7–3 nm; manuscript in preparation), consistent with literature descriptions of unmodified dsRNA (~0.28-nm helical rise/base pair or R_h ~2.9 nm for 21-mer siRNA). As it tumbles freely in solution, 21-mer siRNA R_h is roughly equivalent to a 48 kDa protein (Kok and Rudin, 1981; Wilkins et al., 1999). This conservative

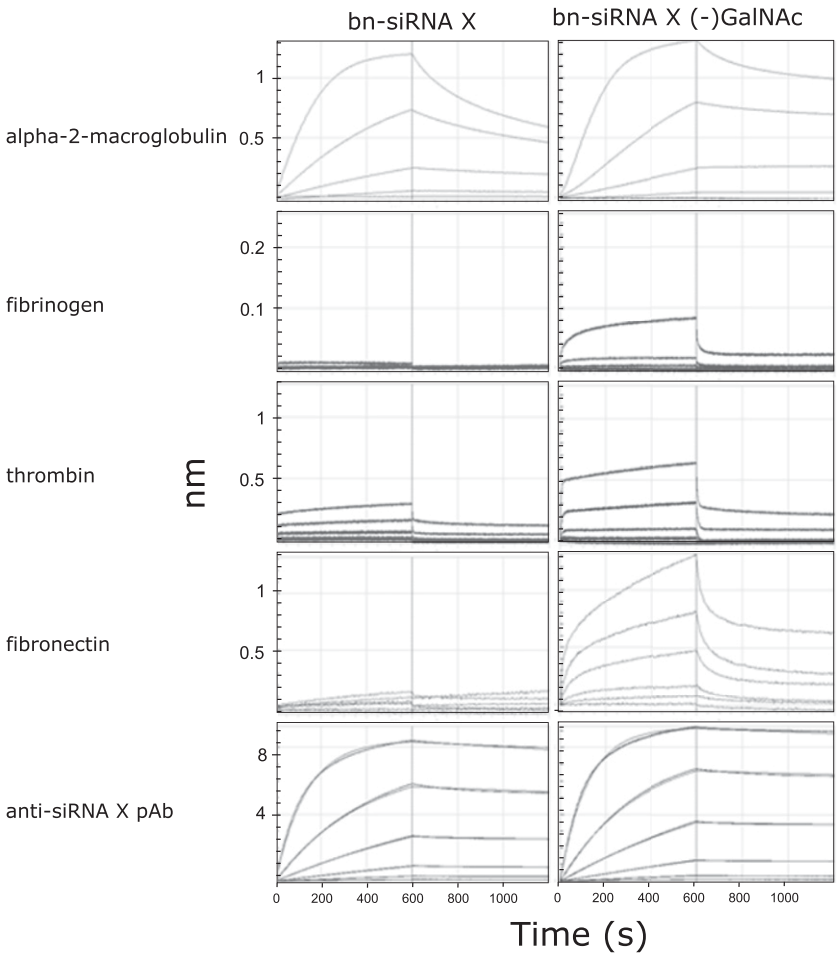

Fig. 5. BLI sensorgrams of positive screening hits for select human plasma proteins binding to biotinylated siRNA-X ± GalNAc. A side-by-side comparison of anti-siRNA pAb (positive control), α-2-macroglobulin, α-thrombin, fibrinogen, and fibronectin binding to bn-siRNA-X with (left column) or without (right column) GalNAc conjugation. Titrations were 1:2 dilutions with a top concentration of 0.5 μM (except pAb = 0.2 μM).

estimate does not account for terminally positioned triantennary GalNAc or cation concentration and identity [(shown for DNA (Fujimoto et al., 1994)]. 2′-F, 2′-OMe, and PS modifications likely do not alter the A-form helical properties (Smith and Nikonowicz, 2000; Liu et al., 2011). Consequently, our recovery data (Table 1) support the siRNA rigid rod hypothesis.

An important implication of siRNA R_h elucidation is that certain organs in the body, including the kidney and lymph nodes, use filtration as a means of sorting molecules. Based on our findings, we recommend using R_h-corrected MW to aid predictions of how these tissues process siRNA.

Application of Protein-Binding Data to Interpret PK-PD Profiles. PPB and liver protein-binding f_u values for siRNA-X at equilibrium are not particularly informative in isolation, as they do not address interaction dynamics and binding affinities in whole blood or at the site of action (e.g., liver). The true value of f_u measurements lies in how they can be applied to interpret the corresponding in vivo PK and PD data. Typical serum half-lives for GalNAc siRNA range from 2 to 8 hours; in contrast, target mRNA knockdown can last from weeks to months (Nair et al., 2017). Such rapid clearance from blood would suggest that a majority of the observed 85%–95% siRNA-X bound to proteins at equilibrium is only transiently bound with rapid dissociation rates (k_{off}). Consequently, if siRNA-X exhibits high affinity for any plasma proteins at all, these hypothetical proteins could only exist at low concentrations (<<37 nM was the lowest PPB concentration tested). An important implication of this scenario is that tightly bound siRNA-X could compete with endogenous ligands or otherwise interfere with physiologic processes of low-abundance plasma proteins.

As the GalNAc-siRNA chemistry repertoire continues to evolve, we advocate that the relationship between PPB and blood PK continue to be monitored, as changes in the identities of GalNAc-siRNA protein-binding partners and/or their affinities could lead to alterations in the distribution and exposure of the molecule, or adverse effects due to interference with endogenous processes. Moreover, understanding the blood distribution, including protein-binding partners, may be beneficial in defining strategies for extrahepatic delivery.

High-affinity ASO binding to specific plasma proteins (nanomolar; via fluorescence polarization) has directly impacted PD in knockout (α-2-macroglobulin) or knockdown (histidine-2-glycoprotein) mice (Shemesh et al., 2016; Gaus et al., 2018). In both cases, protein removal from circulation resulted in a 2-fold ASO activity increase, suggesting protein binding can modulate shunting to unproductive pathways. Although outside the scope of this paper, this experimental approach will aid understanding of the impact of protein binding on siRNA PD.

Given that GalNAc siRNA is delivered to the liver via rapid ASGPR uptake, understanding siRNA-protein interactions at the site of action may aid understanding of the long duration of response. Our findings indicate siRNA is highly bound in the liver at equilibrium. If the binding turns out to be high-affinity, this could confirm the existence of a protein-bound "depot"—with gradual release of siRNA to RISC. Other prevailing theories suggest that the "depot" is a subcellular organelle like the endosome (Dominska and Dykxhoorn, 2010; Juliano and Carver, 2015) or a consequence of RISC-mediated RNA interference being a catalytic process with a long-lived Ago2-siRNA or Ago2-antisense complex (Okamura

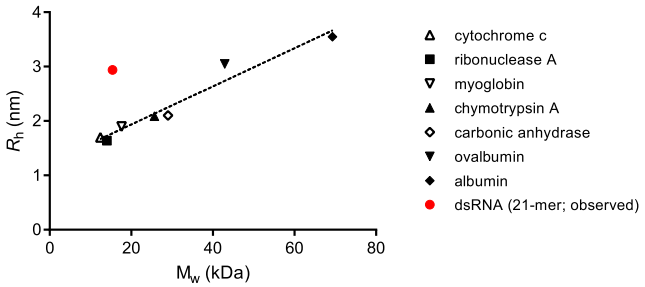

Fig. 6. The relationship between R_h and MW for globular proteins does not hold for the dsRNA linear polymer according to R_h prediction based on dsRNA helical rise and the "siRNA rigid rod" assumption. siRNA is marked in red. GalNAc was not included in the R_h calculation. Linear regression was performed on the protein subset to estimation of the MW for a protein with an equivalent R_h to siRNA. The equation of the line obtained (with siRNA omitted) was y = 0.03509x + 1.233, and this was used to calculate the siRNA-protein MW equivalence value of 48 kDa (GraphPad Prism; calculations provided in Supplemental Calculations 2).

et al., 2004; Wang et al., 2009; Nakanishi, 2016). Consequently, the contribution of liver protein binding to GalNAc siRNA remains an open question.

Toward siRNA PPB Engineering. Aligned with other published oligonucleotide data, our structure-activity relationship data suggest that siRNA PPB is "tunable" (Cossum et al., 1993; Braasch et al., 2004; Watanabe et al., 2006) (Fig. 4). In our limited study looking at the effect of various common chemical modifications, we established that $f_{u,plasma}$ is manipulatable from 0.01 to 0.21 f_u at minimum. Whether binding modulation alters pharmacologic outcome remains to be seen. Modulation strategies might include minimizing binding to toxicity-related proteins, reducing drug-drug interaction liabilities, or targeting binding to specific proteins to facilitate siRNA delivery. For example, diacyl-conjugated siRNA displaying albumin binding demonstrated an increased circulation half-life compared with non-conjugated siRNA (Sarett et al., 2017). More generally, therapeutics directly conjugated to albumin or IgG-containing moieties have prolonged circulatory half-lives due to engagement with the recycling neonatal Fc receptor and reduced kidney filtration (Robbie et al., 2013; Larsen et al., 2018). Other siRNA features currently under investigation that could be exploited for protein-binding modulation include linker chemistry and conjugation to lipophilic molecules, peptides, monoclonal antibodies, or siRNA oligomers (Smith and Nikonowicz, 2000; Khan et al., 2016; Gandioso et al., 2017; Tushir-Singh, 2017).

Developing a standardized assessment of what makes a specific siRNA-protein interaction "meaningful" and characterizing protein-siRNA interactions in terms of specificity and affinity remains an active area of research. While we demonstrated that surfaced-based binding assays have utility in qualitatively identifying siRNA-binding partners (Fig. 5), we also observed significant orientation effects that are likely steric-driven (Supplemental Figs. 4 and 5). In the future, to better rank-order molecules by binding affinity, solution-based equilibrium measurements such as fluorescence polarization [recently applied to ASOs (Gaus et al., 2018)] or kinetic exclusion assays are recommended. To identify novel binders, rather than use a bottom-up approach such as the one performed here using purified proteins of interest, siRNA-protein pull-down combined with mass spectrometry proteomics will provide a nonbiased, comprehensive assessment of the siRNA-protein-binding landscape. To delineate complex relationships between siRNA structure, protein binding, and pharmacological effect, additional studies addressing variation in sequence, chemical modification, modification pattern, and conjugation ligands are needed.

siRNA-Protein Interactions: Changing the Binding Paradigm in a Therapeutic Context. siRNA-protein interactions depend upon numerous factors, including protein structure, siRNA sequence and chemical modifications, kinetics, and concentration. In biologic matrices, additional considerations apply, including competition with other proteins for siRNA binding and competition with other oligonucleotides for protein binding. Affinities between chemically modified therapeutic oligonucleotides and specific proteins range from low nM to >500 μM (Gaus et al., 2018). Due to these complexities, siRNA-protein interactions are not well understood, and they cannot currently be anticipated a priori. To advance siRNA therapeutics, a paradigm shift in experimental design and interpretation is needed.

Rather than conforming to small-molecule-like "lock and key" or "induced fit" principles (Koshland, 1995) or protein-protein interactions, where a certain threshold of specificity and stability is required to achieve meaningful binding (Vishwanath et al., 2017), siRNA-protein interactions are governed by multiple weak complementary forces. These forces are effectively enhanced by the high surface area and high surface area-to-density ratio of siRNA relative to other therapeutic modalities. They include electrostatic and hydrophobic interactions, hydrogen bonding, and base stacking (Luscombe et al., 2001; Jayaram and Jain, 2004; Tolstorukov et al., 2004; Koh et al., 2011). The consequences are complex binding events arising from a convolution of association and dissociation rates, reflecting a distribution of local affinities driven by chemical modification pattern, GalNAc or other conjugate, 5′ phosphorylation state, or 3′ base identity, blurring boundaries of how we think about interaction specificity (Jankowsky and Harris, 2015). Thus, to advance understanding of siRNA-protein interactions in a therapeutic setting, establishment of a new metric of what constitutes a "relevant" binding event in the context of PK-PD analysis is required.

A central rationale guiding us in this work has been to address the following question: Does PPB matter for therapeutic siRNA? In establishing an f_u assay to measure siRNA PPB and liver protein binding, and in developing an siRNA-protein interaction screening platform, we have established a bioanalytical toolkit to build knowledge in this understudied domain. In the future, the in vitro techniques described here can aid in vivo PK-PD data interpretation for this emerging modality and guide design of the next generation of siRNA therapeutics.

Acknowledgments

Thank you to Christina Shen, Ben Jiang, Yun Ling, Zhican Wang, Justin Murray, Babak Basiri, and Fang Xie for their work supporting aspects of this project.

Authorship Contributions

Participated in research design: Humphreys, Rock, Lade, Thayer, Smith.

Conducted experiments: Humphreys, Lade, Basiri, Hao, Huang.

Contributed new reagents or analytic tools: Wu, Sham, Thayer, Basiri, Hao, Huang.

Performed data analysis: Humphreys, Lade.

Wrote or contributed to the writing of the manuscript: Humphreys, Thayer, Lade, Rock, Smith.

References

Allerson CR, Sioufi N, Jarres R, Prakash TP, Naik N, Berdeja A, Wanders L, Griffey RH, Swayze EE, and Bhat B (2005) Fully 2′-modified oligonucleotide duplexes with improved in vitro potency and stability compared to unmodified small interfering RNA. *J Med Chem* **48**:901–904.

Anderson NL and Anderson NG (2002) The human plasma proteome: history, character, and diagnostic prospects [published correction appears in *Mol Cell Proteomics* (2003) 2:50]. *Mol Cell Proteomics* **1**:845–867.

Baeyens KJ, De Bondt HL, and Holbrook SR (1995) Structure of an RNA double helix including uracil-uracil base pairs in an internal loop. *Nat Struct Biol* **2**:56–62.
Bailey JK, Shen W, Liang X-H, and Crooke ST (2017) Nucleic acid binding proteins affect the subcellular distribution of phosphorothioate antisense oligonucleotides. *Nucleic Acids Res* **45**: 10649–10671.
Bhandare V and Ramaswamy A (2016) Structural dynamics of human Argonaute2 and its interaction with siRNAs designed to target mutant tdp43. *Adv Bioinforma* **2016**:8792814.
Braasch DA, Paroo Z, Constantinescu A, Ren G, Öz OK, Mason RP, and Corey DR (2004) Biodistribution of phosphodiester and phosphorothioate siRNA. *Bioorg Med Chem Lett* **14**: 1139–1143.
Brown DA, Kang SH, Gryaznov SM, DeDionisio L, Heidenreich O, Sullivan S, Xu X, and Nerenberg MI (1994) Effect of phosphorothioate modification of oligodeoxynucleotides on specific protein binding. *J Biol Chem* **269**:26801–26805.
Choung S, Kim YJ, Kim S, Park H-O, and Choi Y-C (2006) Chemical modification of siRNAs to improve serum stability without loss of efficacy. *Biochem Biophys Res Commun* **342**:919–927.
Corzo J (2006) Time, the forgotten dimension of ligand binding teaching. *Biochem Mol Biol Educ* **34**:413–416.
Cossum PA, Sasmor H, Dellinger D, Truong L, Cummins L, Owens SR, Markham PM, Shea JP, and Crooke S (1993) Disposition of the 14C-labeled phosphorothioate oligonucleotide ISIS 2105 after intravenous administration to rats. *J Pharmacol Exp Ther* **267**:1181–1190.
Dandekar P, Jain R, Keil M, Loretz B, Koch M, Wenz G, and Lehr CM (2015) Enhanced uptake and siRNA-mediated knockdown of a biologically relevant gene using cyclodextrin polyrotaxane. *J Mater Chem B Mater Biol Med* **3**:2590–2598.
Deitchman AN, Singh RSP, and Derendorf H (2018) Nonlinear protein binding: not what you think. *J Pharm Sci* **107**:1754–1760.
Dominska M and Dykxhoorn DM (2010) Breaking down the barriers: siRNA delivery and endosome escape. *J Cell Sci* **123**:1183–1189.
Foster DJ, Brown CR, Shaikh S, Trapp C, Schlegel MK, Qian K, Sehgal A, Rajeev KG, Jadhav V, Manoharan M, et al. (2018) Advanced siRNA designs further improve in vivo performance of GalNAc-siRNA conjugates. *Mol Ther* **26**:708–717.
Fujimoto BS, Miller JM, Ribeiro NS, and Schurr JM (1994) Effects of different cations on the hydrodynamic radius of DNA. *Biophys J* **67**:304–308.
Gandioso A, Massaguer A, Villegas N, Salvans C, Sánchez D, Brun-Heath I, Marchán V, Orozco M, and Terrazas M (2017) Efficient siRNA-peptide conjugation for specific targeted delivery into tumor cells. *Chem Commun (Camb)* **53**:2870–2873.
Gaus HJ, Gupta R, Chappell AE, Østergaard ME, Swayze EE, and Seth PP (2018) Characterization of the interactions of chemically-modified therapeutic nucleic acids with plasma proteins using a fluorescence polarization assay. *Nucleic Acids Res* DOI: 10.1093/nar/gky1260 [published ahead of print].
Geary RS, Norris D, Yu R, and Bennett CF (2015) Pharmacokinetics, biodistribution and cell uptake of antisense oligonucleotides. *Adv Drug Deliv Rev* **87**:46–51.
Hoy SM (2018) Patisiran: first global approval. *Drugs* **78**:1625–1631.
Hughes TP, Pickels EG, and Horsfall FL (1938) A method for determining the differential sedimentation of proteins in the high speed concentration centrifuge. *J Exp Med* **67**:941–952.
Janas MM, Schlegel MK, Harbison CE, Yilmaz VO, Jiang Y, Parmar R, Zlatev I, Castoreno A, Xu H, Shulga-Morskaya S, et al. (2018) Selection of GalNAc-conjugated siRNAs with limited off-target-driven rat hepatotoxicity. *Nat Commun* **9**:723.
Jankowsky E and Harris ME (2015) Specificity and nonspecificity in RNA-protein interactions. *Nat Rev Mol Cell Biol* **16**:533–544.
Jayaram B and Jain T (2004) The role of water in protein-DNA recognition. *Annu Rev Biophys Biomol Struct* **33**:343–361.
Juliano RL (2016) The delivery of therapeutic oligonucleotides. *Nucleic Acids Res* **44**:6518–6548.
Juliano RL and Carver K (2015) Cellular uptake and intracellular trafficking of oligonucleotides. *Adv Drug Deliv Rev* **87**:35–45.
Kalvass JC, Maurer TS, and Pollack GM (2007) Use of plasma and brain unbound fractions to assess the extent of brain distribution of 34 drugs: comparison of unbound concentration ratios to in vivo p-glycoprotein efflux ratios. *Drug Metab Dispos* **35**:660–666.
Khan T, Weber H, DiMuzio J, Matter A, Dogdas B, Shah T, Thankappan A, Disa J, Jadhav V, Lubbers L, et al. (2016) Silencing myostatin using cholesterol-conjugated siRNAs induces muscle growth. *Mol Ther Nucleic Acids* **5**:e342.
Koh YY, Wang Y, Qiu C, Opperman L, Gross L, Tanaka Hall TM, and Wickens M (2011) Stacking interactions in PUF-RNA complexes. *RNA* **17**:718–727.
Kok CM and Rudin A (1981) Relationship between the hydrodynamic radius and the radius of gyration of a polymer in solution. *Makromol Chem Rapid Commun* **2**:655–659.
Kornyshev AA and Leikin S (2013) Helical structure determines different susceptibilities of dsDNA, dsRNA, and tsDNA to counterion-induced condensation. *Biophys J* **104**:2031–2041.
Koshland DE (1995) The key–lock theory and the induced fit theory. *Angew Chem Int Ed Engl* **33**: 2375–2378.
Kozielski KL, Tzeng SY, and Green JJ (2013) Bioengineered nanoparticles for siRNA delivery. *Wiley Interdiscip Rev Nanomed Nanobiotechnol* **5**:449–468.
Larsen MT, Rawsthorne H, Schelde KK, Dagnæs-Hansen F, Cameron J, and Howard KA (2018) Cellular recycling-driven in vivo half-life extension using recombinant albumin fusions tuned for neonatal Fc receptor (FcRn) engagement. *J Control Release* **287**:132–141.
Liu J, Guo S, Cinier M, Shlyakhtenko LS, Shu Y, Chen C, Shen G, and Guo P (2011) Fabrication of stable and RNase-resistant RNA nanoparticles active in gearing the nanomotors for viral DNA packaging. *ACS Nano* **5**:237–246.
Long SB, Long MB, White RR, and Sullenger BA (2008) Crystal structure of an RNA aptamer bound to thrombin. *RNA* **14**:2504–2512.
Luscombe NM, Laskowski RA, and Thornton JM (2001) Amino acid-base interactions: a three-dimensional analysis of protein-DNA interactions at an atomic level. *Nucleic Acids Res* **29**: 2860–2874.
Nair JK, Attarwala H, Sehgal A, Wang Q, Aluri K, Zhang X, Gao M, Liu J, Indrakanti R, Schofield S, et al. (2017) Impact of enhanced metabolic stability on pharmacokinetics and pharmacodynamics of GalNAc-siRNA conjugates. *Nucleic Acids Res* **45**:10969–10977.
Nakanishi K (2016) Anatomy of RISC: how do small RNAs and chaperones activate Argonaute proteins? *Wiley Interdiscip Rev RNA* **7**:637–660.
Okamura K, Ishizuka A, Siomi H, and Siomi MC (2004) Distinct roles for Argonaute proteins in small RNA-directed RNA cleavage pathways. *Genes Dev* **18**:1655–1666.
O'Reilly RA (1972) Sodium warfarin. *Pharmacology* **8**:181–190.
Pfeifer ND, Harris KB, Yan GZ, and Brouwer KL (2013) Determination of intracellular unbound concentrations and subcellular localization of drugs in rat sandwich-cultured hepatocytes compared with liver tissue. *Drug Metab Dispos* **41**:1949–1956.
Robbie GJ, Criste R, Dall'acqua WF, Jensen K, Patel NK, Losonsky GA, and Griffin MP (2013) A novel investigational Fc-modified humanized monoclonal antibody, motavizumab-YTE, has an extended half-life in healthy adults. *Antimicrob Agents Chemother* **57**:6147–6153.
Rowland M, Tozer TN, and Rowland M (2011) *Clinical Pharmacokinetics and Pharmacodynamics: Concepts and Applications*, Wolters Kluwer Health/Lippincott William & Wilkins, Philadelphia.
Sarett SM, Werfel TA, Lee L, Jackson MA, Kilchrist KV, Brantley-Sieders D, and Duvall CL (2017) Lipophilic siRNA targets albumin in situ and promotes bioavailability, tumor penetration, and carrier-free gene silencing. *Proc Natl Acad Sci USA* **114**:E6490–E6497.
Schirle NT, Kinberger GA, Murray HF, Lima WF, Prakash TP, and MacRae IJ (2016) Structural analysis of human argonaute-2 bound to a modified siRNA guide. *J Am Chem Soc* **138**: 8694–8697.
Schmidt S, Gonzalez D, and Derendorf H (2010) Significance of protein binding in pharmacokinetics and pharmacodynamics. *J Pharm Sci* **99**:1107–1122.
Shemesh CS, Yu RZ, Gaus HJ, Seth PP, Swayze EE, Bennett FC, Geary RS, Henry SP, and Wang Y (2016) Pharmacokinetic and pharmacodynamic investigations of ION-353382, a model antisense oligonucleotide: using alpha-2-macroglobulin and murinoglobulin double-knockout mice. *Nucleic Acid Ther* **26**:223–235.
Shen W, Liang XH, Sun H, and Crooke ST (2015) 2′-Fluoro-modified phosphorothioate oligonucleotide can cause rapid degradation of P54nrb and PSF. *Nucleic Acids Res* **43**:4569–4578.
Smith JS and Nikonowicz EP (2000) Phosphorothioate substitution can substantially alter RNA conformation. *Biochemistry* **39**:5642–5652.
Springer AD and Dowdy SF (2018) GalNAc-siRNA conjugates: leading the way for delivery of RNAi therapeutics. *Nucleic Acid Ther* **28**:109–118.
Srinivasan SK, Tewary HK, and Iversen PL (1995) Characterization of binding sites, extent of binding, and drug interactions of oligonucleotides with albumin. *Antisense Res Dev* **5**:131–139.
Taylor P, Rixon F, and Desselberger U (1985) Rise per base pair in helices of double-stranded rotavirus RNA determined by electron microscopy. *Virus Res* **2**:175–182.
Tolstorukov MY, Jernigan RL, and Zhurkin VB (2004) Protein-DNA hydrophobic recognition in the minor groove is facilitated by sugar switching. *J Mol Biol* **337**:65–76.
Tushir-Singh J (2017) Antibody-siRNA conjugates: drugging the undruggable for anti-leukemic therapy. *Expert Opin Biol Ther* **17**:325–338.
Ulrich H, Magdesian MH, Alves MJM, and Colli W (2002) In vitro selection of RNA aptamers that bind to cell adhesion receptors of Trypanosoma cruzi and inhibit cell invasion. *J Biol Chem* **277**: 20756–20762.
Vickers TA and Crooke ST (2016) Development of a quantitative BRET affinity assay for nucleic acid-protein interactions. *PLoS One* **11**:e0161930.
Vishwanath S, Sukhwal A, Sowdhamini R, and Srinivasan N (2017) Specificity and stability of transient protein-protein interactions. *Curr Opin Struct Biol* **44**:77–86.
Wang H-W, Noland C, Siridechadilok B, Taylor DW, Ma E, Felderer K, Doudna JA, and Nogales E (2009) Structural insights into RNA processing by the human RISC-loading complex. *Nat Struct Mol Biol* **16**:1148–1153.
Watanabe TA, Geary RS, and Levin AA (2006) Plasma protein binding of an antisense oligonucleotide targeting human ICAM-1 (ISIS 2302). *Oligonucleotides* **16**:169–180.
Wilce J, Vivian J, and Wilce M (2012) Oligonucleotide binding proteins, in *Protein Dimerization and Oligomerization in Biology* (Matthews JM ed) pp 91–104, Springer, New York.
Wilkins DK, Grimshaw SB, Receveur V, Dobson CM, Jones JA, and Smith LJ (1999) Hydrodynamic radii of native and denatured proteins measured by pulse field gradient NMR techniques. *Biochemistry* **38**:16424–16431.
Yoshikado T, Toshimoto K, Nakada T, Ikejiri K, Kusuhara H, Maeda K, and Sugiyama Y (2017) Comparison of methods for estimating unbound intracellular-to-medium concentration ratios in rat and human hepatocytes using statins. *Drug Metab Dispos* **45**:779–789.
Zeitlinger MA, Derendorf H, Mouton JW, Cars O, Craig WA, Andes D, and Theuretzbacher U (2011) Protein binding: do we ever learn? *Antimicrob Agents Chemother* **55**:3067–3074.

Address correspondence to: Sara C. Humphreys, Department of Pharmacokinetics and Drug Metabolism, 1120 Veterans Boulevard, South San Francisco, CA 94080. E-mail: shumph01@amgen.com

Supplemental Material

Drug Metabolism and Disposition

Plasma and liver protein binding of GalNAc conjugated siRNA

Sara. C. Humphreys[1*], Mai B. Thayer[1], Julie M. Lade[1], Bin Wu[2], Kelvin Sham[2], Babak Basiri[1], Yue Hao[3], Xin Huang[3], Richard Smith[1] and Brooke M. Rock[1]

[1]Pharmacokinetics and Drug Metabolism Department, Amgen Research, 1120 Veterans Boulevard, South San Francisco, CA, 94080, USA

[2]Hybrid Modality Engineering Department, Amgen Research, One Amgen Center Drive, Thousand Oaks, CA, 91320, USA

[3]Molecular Engineering Department, Amgen Research, 360 Binney Street, Cambridge, MA, 02141, USA

*Corresponding author

Supplemental Methods

Recovery of siRNA-X in PBST by 20 MWCO equilibrium dialysis

Device Preparation: Pre-soak Slide-A-Lyzer 20 kDa MWCO equilibrium dialysis units in a large volume of PBST for 2 hours, then replace the buffer and leave overnight. Immediately prior to use, pick up device with tweezers and tap vigorously to remove excess liquid.

Sample Preparation: Add 100 µL siRNA-X spiked in PBST to each device. Place in receiver chamber containing 1.8 mL PBST and leave to equilibrate overnight at 37°C, shaking at 500 rpm. Once at equilibrium, remove device, thoroughly mix sample in receiver.

siRNA Detection and Quantitation: By hybridization ELISA (see main body).

Results: ultrafiltration siRNA-X recovery in buffer is reported in Table 1.

Recovery of siRNA-X in PBST by ultracentrifugation

Sample Preparation: siRNA working stocks were prepared in 1x PBS and added to PBST buffer for a final concentration of 1 µM. Following an equilibration for 15 min at 37°C, each sample (200 µL) was transferred to polycarbonate tubes (7 x 20 mm) in triplicate and centrifuged at 390,880 *x*g for 3 hours at 37°C using an Optima TLX Ultracentrifuge (Beckman Coulter). After centrifugation, 50 µL of supernatant (3 h) was removed for recovery analysis.

siRNA Detection and Quantitation: Samples were diluted 1:10 in hybridization ELISA sample buffer for siRNA quantitation. The final recovered fraction was calculated using the following equation:

$$Unbound\ fraction = \frac{Ultracentrifuge\ supernatant\ at\ 3\ h}{Spiked\ buffer\ at\ 0\ h}$$

Results: Ultracentrifugation siRNA-X recovery in buffer experiments are reported in Table 1.

Recovery of siRNA-X, siRNA-Y and siRNA-Z in PBS+CHAPS by ultrafiltration

To compare 50 MWCO ultrafiltration recovery using PBST and PBS+CHAPS (0.1% (w/v) CHAPS), we repeated the recovery experiment described in the Methods section, replacing PBST with PBS+CHAPS for filter pre-treatment and for siRNA spikes (1 µM siRNA-X, siRNA-Y and siRNA-Z; structural topology of each of these molecules is depicted in Supplemental Figure 3).

Small molecule $f_{u,plasma}$ *and* $f_{u,liver}$ ultracentrifugation method

Neat pooled and mixed gender human plasma was titrated to a pH of 7.2-7.4. Antipyrine and timolol working stocks were prepared in 1x PBS and added to plasma for a final concentration of 1.0 µM. Rosuvastatin was similarly prepared in liver homogenate. Following equilibration for 15 minutes at 37°C, each suspension (200 µL) was transferred to polycarbonate tubes (7 × 20 mm) in triplicate and centrifuged at 390,880 *x*g for 3 h at 37°C using an Optima TLX Ultracentrifuge (Beckman Coulter). To facilitate the calculation of fraction unbound, 50 µL of initial spiked plasma suspensions (0 hour) were added in triplicate to 50µL plasma ultrafiltrate for each respective species. After centrifugation, 50 µL of supernatant (3 hours) was removed and added to plasma ultrafiltrate. Samples were diluted 1:10 in hybridization-ligation sample buffer for siRNA quantitation via LC-MS/MS. The final plasma unbound fraction was calculated by dividing the small molecule signal in the ultracentrifuge supernatant by the spiked plasma at 0 hours. Results are reported in Table 2.

EMSA of siRNA-plasma 50 MWCO ultrafiltrate

Part I: EMSA to investigate siRNA-protein binding in the ultrafiltrate

Sample preparation: Add 4 µL ultrafiltrate (receiver compartment) or spiked plasma (donor compartment) to 20 µL 1× sample buffer (Novex Hi-Density TBE Sample Buffer (Thermo Fisher, #LC6678)), load 5 µL onto a 20% PAGE gel and run at 200 V. Stain with SYBR Gold according to the manufacturer's instructions (Thermo Fisher, #S11494) and image using UV transillumination.

Data analysis: Visual comparison

Results: Supplemental Figure 2A shows two major SYBR Gold-staining bands in the plasma ultrafiltrate and one band in the buffer control ultrafiltrate. For each siRNA construct, the lower band in the plasma ultrafiltrate corresponds to the band in the buffer control, indicating "unbound" siRNA. We suspected that the upper band corresponded to albumin, which was confirmed in the Supplemental Figure 2B. In Figure S5, we show that albumin does not bind to siRNA-X up to 1 µM, therefore, Supplemental Figure 2A demonstrates that the vast majority of siRNA in the ultrafiltrate is unbound.

PART II: Electrophoretic Mobility Shift Assay to query whether the additional band observed in plasma was associated with albumin

Sample preparation: Perform a 1:1 titration of albumin binding protein (~22 kDa, generated in-house) into 10% human plasma (12 pt + blank; top concentration: 164 µM) in TBE and incubate for 30 min. at 30° C. Load, run, stain and visualize gel as above.

*Results***:** Supplemental Figure 3B shows that a known albumin binding protein (an engineered version of Protein G) was able to displace the putative albumin band in human plasma, thus confirming its identity. Note that in this experiment, no siRNA was present, so albumin itself stains with SYBR Gold, perhaps as the result of some endogenous nucleotide binding. The albumin binding protein did not stain with SYBR Gold (data not shown). The observation that some fraction of albumin gets through the 50 kDa MWCO filter is not too surprising given the high abundance of albumin and plasma and the fact that the 50 kDa MWCO exclusion limit actually represents a distribution of filter pore sizes.

BLI of various siRNA-like constructs to inform understanding of orientation and GalNAc effects in human and rat plasma

Sample Preparation: As for time-to-equilibrium experiments described in Methods section with the exception that a panel of biotinylated siRNA-like constructs were used. The panel included, the anti-sense or the sense strand of siRNA-X hybridized with a complementary fully 2′OMe sequence that was conjugated with biotin at either the 5′ or the 3′ terminus. In addition, we loaded the single-stranded biotinylated fully 2′OMe strands alone. We used rat plasma in addition to human plasma at the same concentrations.

Results: This panel highlighted the effects of orientation, GalNAc conjugation, ds vs. ssRNA, sequence differences, and chemical modification differences (siRNA-X sense and antisense do not have the same chemical modification patterns or composition).

LC-MS analysis: 1.0 µM siRNA was added to 200 µL aliquots of rat plasma either at the beginning or at the end of a 48 hr incubation period at 37°C. Extraction of siRNA from samples was accomplished by utilizing Clarity OTX SPE plates (Phenomenex, Torrance, CA). The LC-MS analysis was performed using an Agilent Technologies (Santa Clara, CA) 1290 Infinity series UPLC system consisting of a binary pump, a refrigerated autosampler and a temperature-controlled column compartment (TCC) coupled to a Thermo Scientific (Waltham, MA) Q Exactive HF-X Orbitrap mass spectrometer. Samples were separated on a Waters (Milford, MA) 2.1 X 50 mm Acquity UPLC Oligonucleotide BEH C18 Column (130 Å, 1.7 µm) at 80°C. Mobile phase A consisted of 15 mM triethylamine (TEA), 400 mM hexafluoroisopropanol (HFIP) in water and mobile phase B was 15 mM TEA, 400 mM HFIP in methanol. 20 µL of each sample was injected at a 0.4 mL/min flow rate under the following gradient condition (min – %B): 0 – 2 , 1.5 – 2 , 11.5 – 60 , 12 – 95 , 14 – 95 , 14.5 – 2 , 15.5 – 2. The total runtime was 16 minutes and the LC output was diverted to waste from 0 – 2 min and 12 – 16 min.

The mass spectrometer was operated with the following parameters: spray voltage (3.2 kV), capillary temperature (320°C), sheath gas flow rate (50 arbitrary units), sweep gas flow rate (1 arbitrary units), auxillary gas flow rate (10 arbitrary units), auxillary gas temperature (425°C), Full scan negative-ion mode with 60,000 resolution. Instrument control and data acquisition was performed using the Xcalibur 4.0 from Thermo Scientific (Waltham, MA). Corresponding extracted ion chromatograms (XICs) were examined for the expected m/z of sense and antisense strands to determine their stability in plasma.

Supplemental Figures

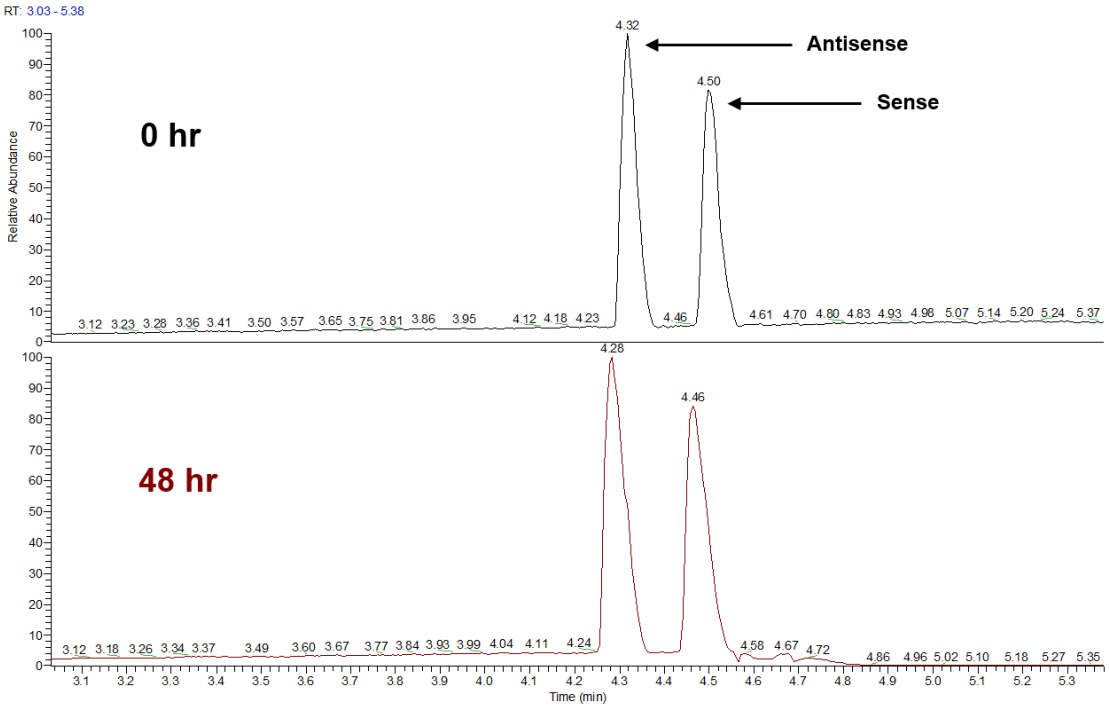

Supplemental Figure 1: Rat plasma stability data of siRNA-X.

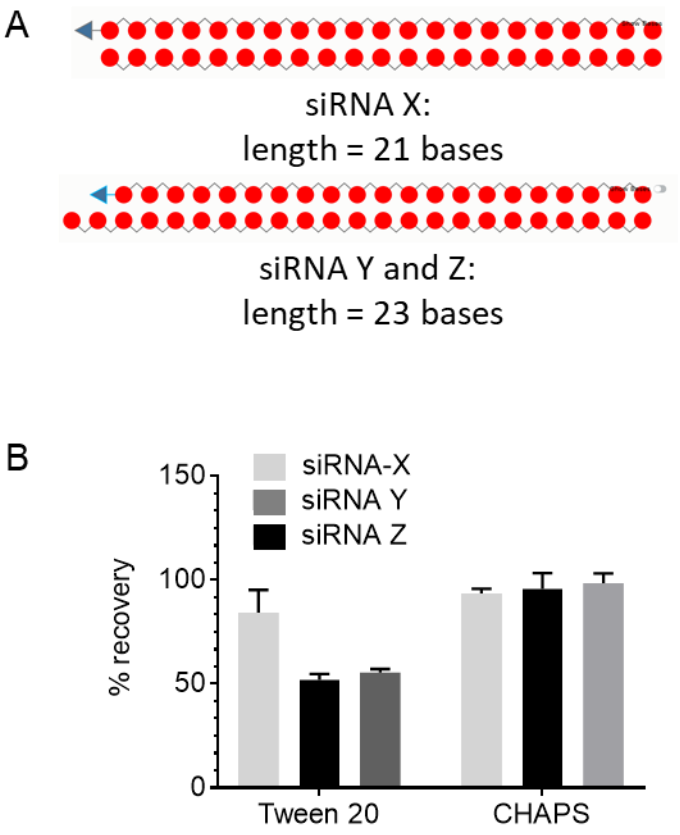

Supplemental Figure 2: The effect of siRNA length and detergent on recovery in buffer via 50 MWCO ultrafiltration. (A) Topographical structural depictions of siRNA-X, siRNA-Y and siRNA-Z. Triantennary GalNAc is depicted as a blue triangle. siRNA-X is a bluntmer containing 2'OMe, 2'F and PS modifications. siRNA-Y and siRNA-Z are asymmetric and contain 2'OMe, 2'F and PS modifications. (B) Recovery in in filters pre-treated with PBST (0.5% Tween-20) or PBS-CHAPS (0.1% CHAPS).

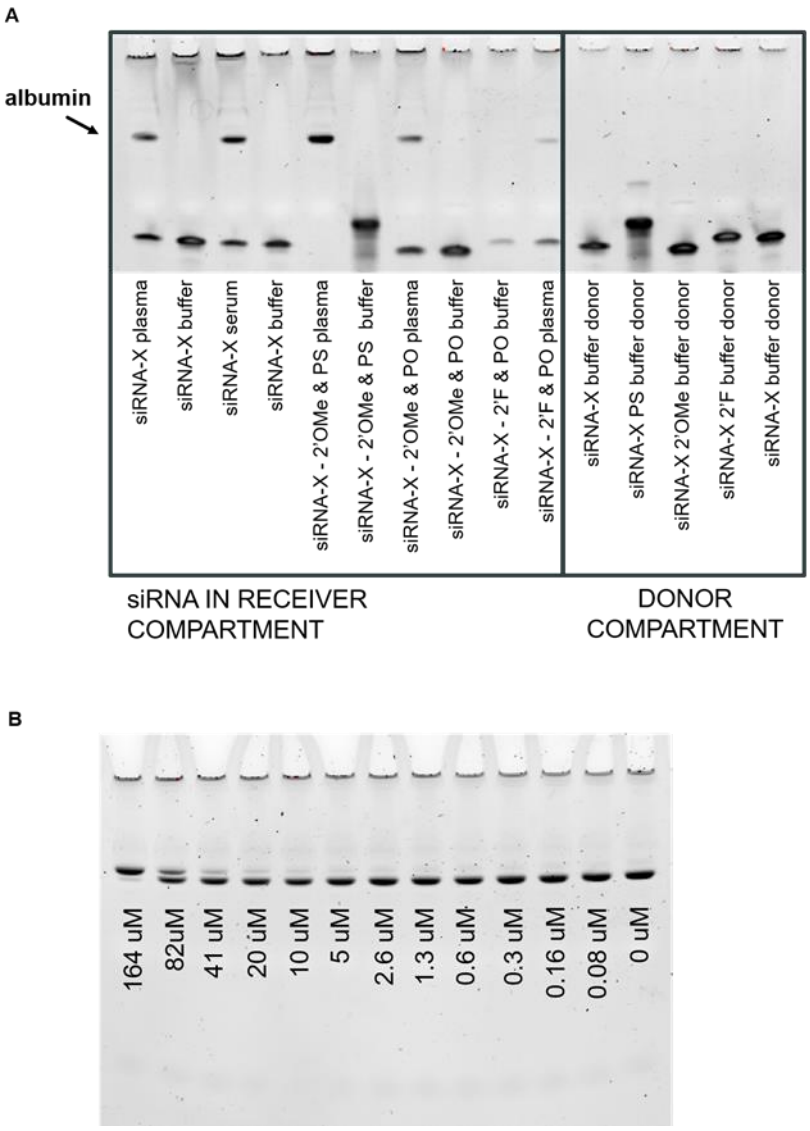

Supplemental Figure 3: The majority of siRNA in the plasma ultrafiltrate after 50 MWCO ultrafiltration is unbound by EMSA. (A) Shows side-by-side plasma and buffer ultrafiltrate recovery of the various siRNA-X constructs shown in Figure 4A. The relative band intensities visually reflect the PPB values reported in Figure 4B. (B) Shows that the upper band in (A) stains with SYBR Gold in the absence of siRNA, and that the band can be displaced with an albumin binding protein.

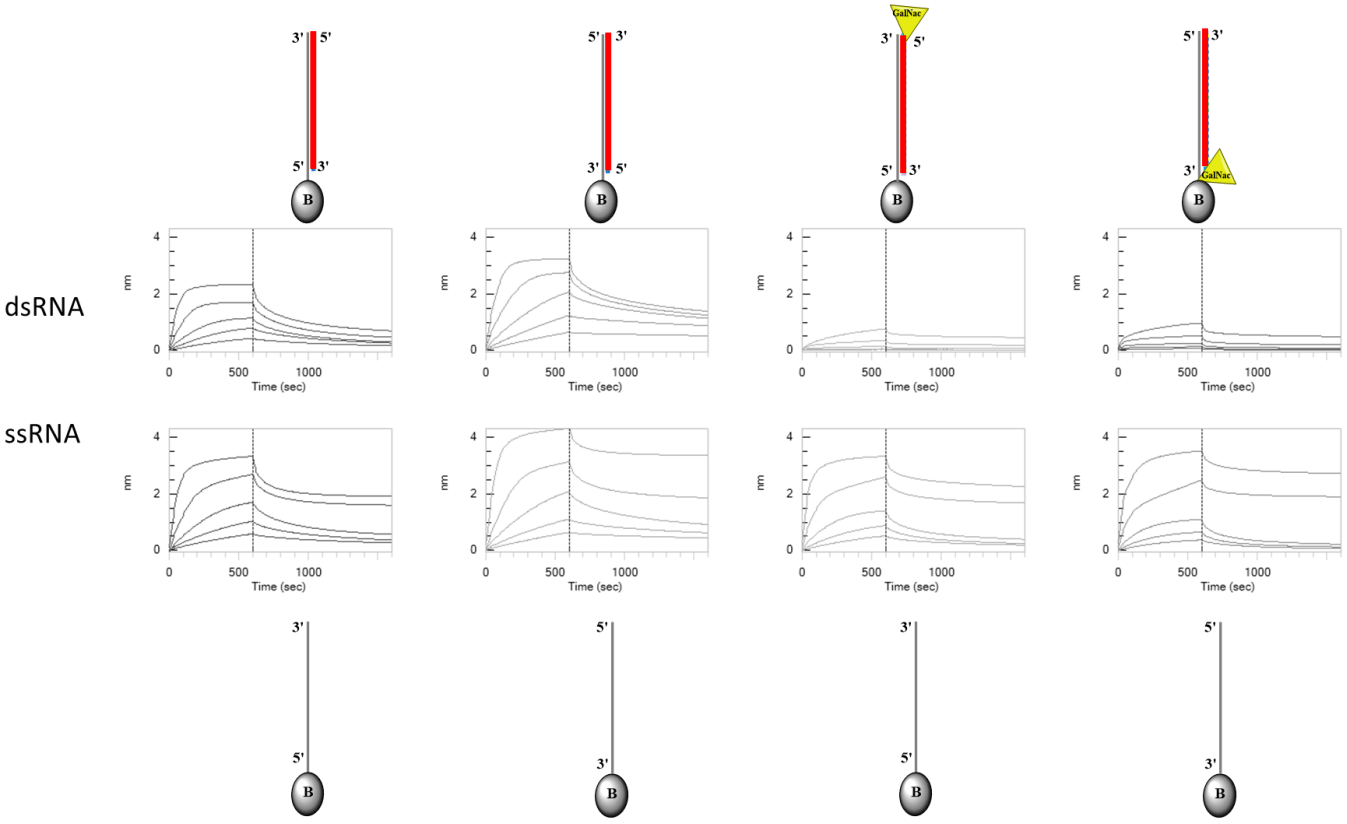

Supplemental Figure 4: Binding of a panel of biotinylated siRNA-X related constructs to a titration of human plasma. TOP ROW: dsRNA constructs with the sense or antisense strand of siRNA-X (colored) hybridized to a biotinylated fully 2'OMe complementary strand. All four possible combinations and orientations loaded as depicted. The yellow triangle represents the GalNAc position when the siRNA-X sense strand is present. BOTTOM ROW: ssRNA versions of what was run on the top row, with "sense-like" 2'OMe sequences on the left and "antisense-like" 2'OMe sequences on the right.

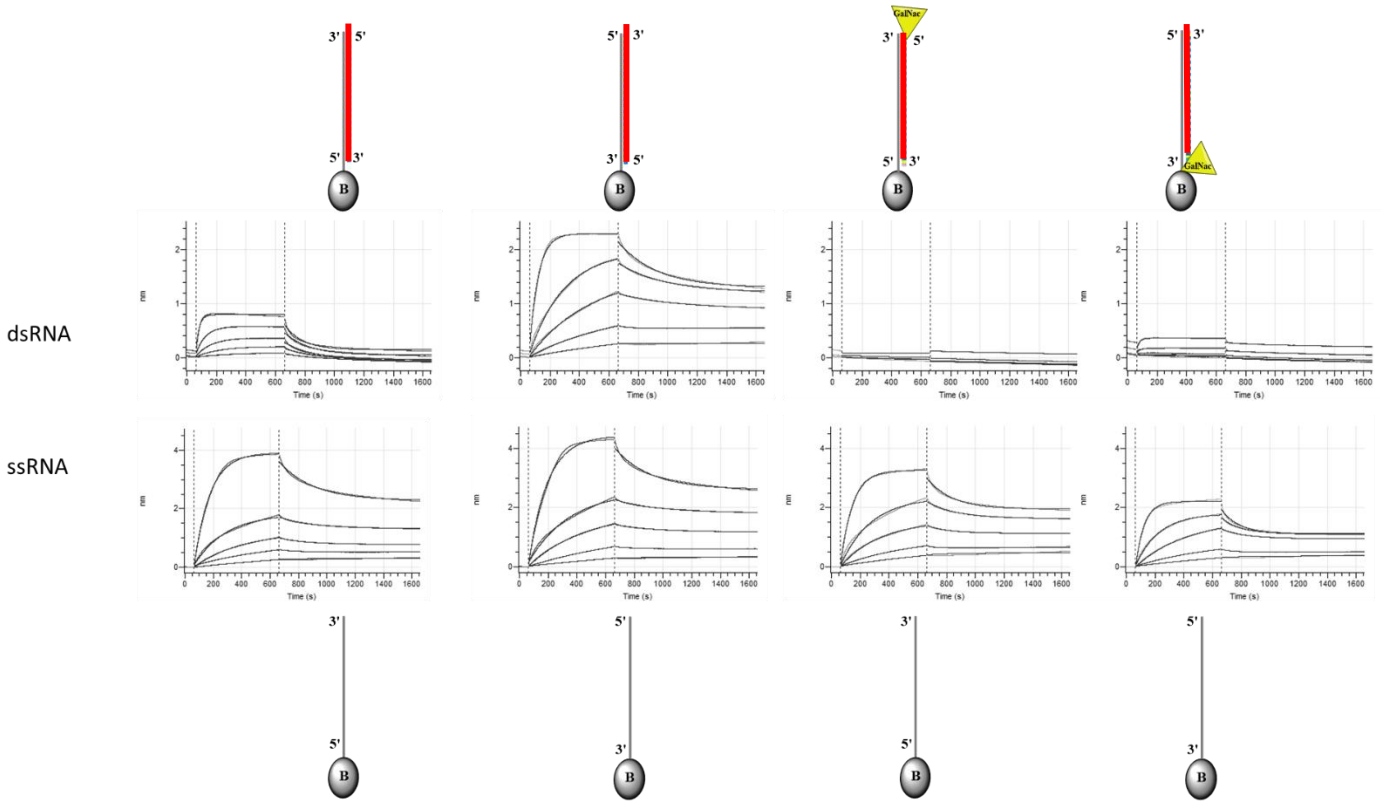

Supplemental Figure 5: Binding of a panel of biotinylated siRNA-X related constructs to a titration of rat plasma. TOP ROW: dsRNA constructs with the sense or antisense strand of siRNA-X (colored) hybridized to a biotinylated fully 2'OMe complementary strand. All four possible combinations and orientations loaded as depicted. The yellow triangle represents the GalNAc position when the siRNA-X sense strand is present. BOTTOM ROW: ssRNA versions of what was run on the top row, with "sense-like" 2'OMe sequences on the left and "antisense-like" 2'OMe sequences on the right.

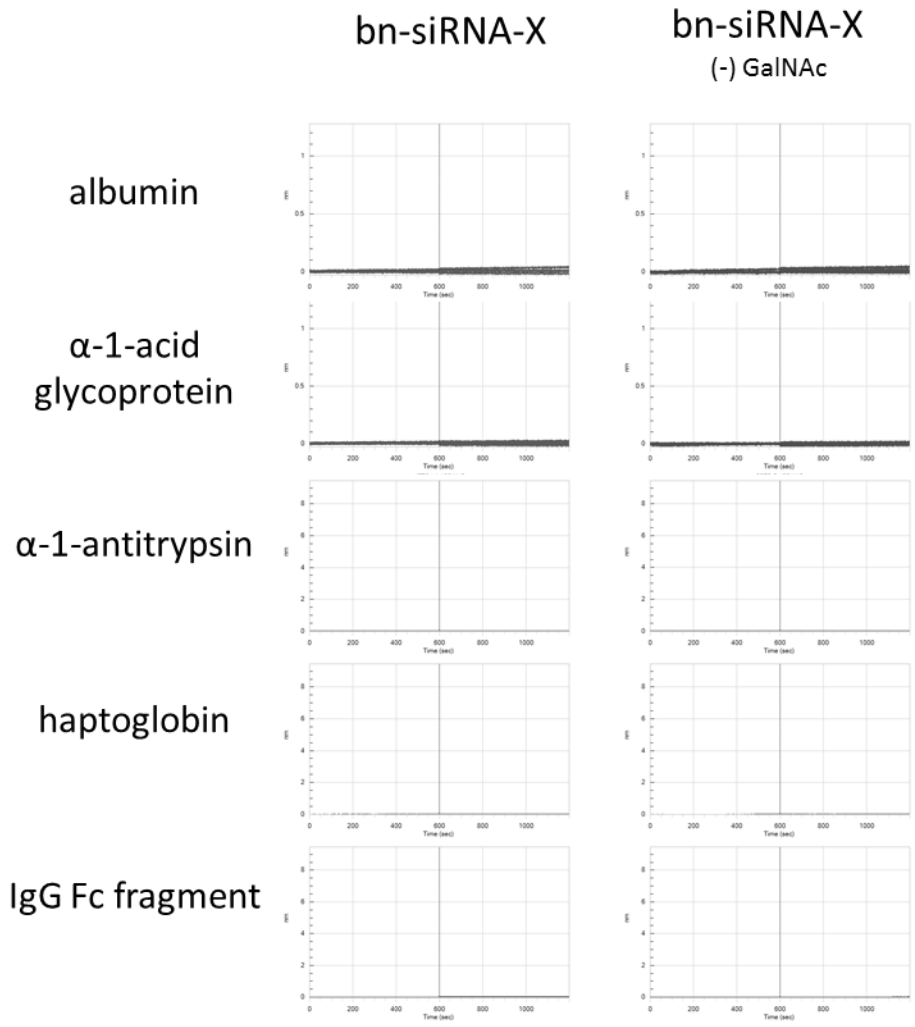

Supplemental Figure 6: negative results of BLI experiment shown in Figure 5. At concentrations up to 1 µM, the following human plasma proteins do not bind to bn-siRNA-X ± GalNAc: albumin, α-1-acid glycoprotein, α-1-antitrypsin, haptoglobin and IgG Fc.

Supplemental Calculation 1: Example R_h calculation

Angstroms per dsRNA helix base-pair (from literature):	2.77 Å/bp
Convert to nanometers:	0.277 nm/bp
Typical number of base-pairs in siRNA:	21
Total length of siRNA:	21 × 0.277 = 5.817 nm
R_h	5.817 nm / 2 = 2.910 nm

Supplemental Calculation 2: M_w (in kDa) estimation for a protein with an equivalent R_h to siRNA

Line equation from linear regression fit of M_w vs R_h (Figure 6)	y = 0.03509x + 1.233
Fix y at 2.910 nm and solve for x	x = (2.910 – 1.233) / 0.03509
	x = 47.8 kDa

Supplemental Discussion

Interpretation of specific siRNA-plasma protein binding interactions

The negative finding for albumin and α1-acid glycoprotein is consistent with a report that less than 2.1% of patisiran, the first and only current FDA-approved siRNA, is bound to these proteins in vitro, however details of the method have not been provided (ONPATTRO™ [patisiran] HIGHLIGHTS OF PRESCRIBING INFORMATION 2018, found at https://www.alnylam.com/wp-content/uploads/2018/08/ONPATTRO-Prescribing-Information.pdf on December 4, 2018). The fact that fibrinogen and fibronectin did not bind to bn-siRNA-X, suggests that these proteins do not bind to GalNAc, and that in this assay format, GalNAc blocks siRNA-X binding. Interestingly, although less siRNA-X protein binding was observed in serum vs. plasma, the difference was not statistically significant, indicating that clotting factors, such as fibrinogen, do not account for a significant proportion of the overall binding observed (Fig. 4).

Given the high concentration of albumin in plasma and serum (530-750 μM (Rustad et al. 2004), it was important for us to understand whether albumin bound to siRNA-X. Our BLI screening assay showed no binding up to 1 μM, meaning that if there is any binding at all, the dissociation constant (K_D), is much greater than 1 μM, and consequently weak, non-specific, and highly transient. We attempted to run this screen at higher concentrations but observed significant solvent-like effects. From the available literature, our finding is consistent with Onishi et al., who found that fully phosphorothioated DNA and locked nucleic acid (LNA) ASOs did not bind to albumin without conjugation to lipophilic ligands using surface plasmon resonance (Onishi et al. 2015); however, it is inconsistent with other groups who showed weak (μM) albumin-ASO interactions with fully phosphorothioated ASOs (Watanabe et al. 2006, Gaus et al. 2018). While these ASO data are potentially informative, again, it is important to remember that ASOs (ssDNA) and siRNA (dsRNA) have very different physicochemical properties and modification patterns likely leading to significant differences in protein binding.

Aside from the pAb, all observed siRNA-protein interactions were highly atypical in that they were multi-phasic and could therefore not be fit to 1:1 binding models. As such, we elected to use the data as a qualitative screen only – assigning sensorgrams as binding "hits" or not. Such screens may be applied in future as a hit-pick based identification of specific siRNA-protein interactions that warrant further investigation. Given the binding complexities observed, we did not attempt to interpret the BLI signal amplitudes for this work. In addition, in performing related studies, we observed significant orientation, strand (double- vs. single-strand), chemical modification type, chemical modification pattern, species, and GalNAc-related orientation effects; all altering the apparent binding affinity of immobilized RNA to plasma proteins (some example sensorgrams provided in Supplemental Figures 4 and 5). This led us to conclude that while surface-based technologies such as BLI provide qualitative insight into whether a protein can bind to RNA, the kinetic data obtained is highly dependent on the method of siRNA immobilization used. To minimize sensorgram complexity, buffer optimization (i.e. changing the pH or salt concentration) may aid to empirically identify more canonical 1:1 binding curves for specific siRNA-protein interactions on a case-by-case basis, however, we advise caution with this approach given that RNA-protein interactions are known to fall along a spectrum ranging from specific to non-specific, and slight buffer alterations could have drastic effects on the apparent affinity and/or number of binding modes (Jankowsky et al. 2015, Gaus et al. 2018). Consequently, the SM- and protein-protein interaction paradigm of globally fitting surfaced-based titrations to 1:1 binding models does not apply to a majority of protein interactions with oligonucleotides such as siRNA.

Finally, although by nature pAbs are heterogenous mixtures – meaning they cannot strictly be fit with 1:1 binding models – we elected to determine the siRNA-pAb kinetic constants to give a sense of what values

to expect for tight, specific, siRNA-protein interactions. By globally fitting the sensorgrams to a 1:1 model, we calculated an apparent K_D (~K_D) of 2.60 ± 0.03 nM, an apparent on rate (~k_{on}) of 3.661 x 10^4 ± 0.006 x 10^4 $M^{-1}.s^{-1}$, and an apparent off rate (~k_{off}) of 9.53 x 10^{-5} ± 0.09 x 10^{-5} s^{-1} (Fig. 5).

References

Gaus, H. J., R. Gupta, A. E. Chappell, M. E. Ostergaard, E. E. Swayze & P. P. Seth (2018) Characterization of the interactions of chemically-modified therapeutic nucleic acids with plasma proteins using a fluorescence polarization assay. *Nucleic Acids Res*.

Jankowsky, E. & M. E. Harris (2015) Specificity and nonspecificity in RNA-protein interactions. *Nat Rev Mol Cell Biol,* 16**,** 533-44.

Onishi, R., A. Watanabe, M. Nakajima, M. Sekiguchi, A. Kugimiya, H. Kinouchi, Y. Nihashi & H. Kamimori (2015) Surface Plasmon Resonance Assay of Binding Properties of Antisense Oligonucleotides to Serum Albumins and Lipoproteins. *Anal Sci,* 31**,** 1255-60.

Rustad, P., P. Felding, L. Franzson, V. Kairisto, A. Lahti, A. Martensson, P. Hyltoft Petersen, P. Simonsson, H. Steensland & A. Uldall (2004) The Nordic Reference Interval Project 2000: recommended reference intervals for 25 common biochemical properties. *Scand J Clin Lab Invest,* 64**,** 271-84.

Watanabe, T. A., R. S. Geary & A. A. Levin (2006) Plasma protein binding of an antisense oligonucleotide targeting human ICAM-1 (ISIS 2302). *Oligonucleotides,* 16**,** 169-80.